



Catalytic combustion of chlorinated aromatics over WO_x/CeO_2 catalysts at low temperature



Yufeng Gu^a, Ting Cai^b, Xiaohui Gao^a, Hangqi Xia^a, Wei Sun^a, Jian Zhao^a, Qiguang Dai^a, Xingyi Wang^{a,*}

^a Lab for Advanced Materials, Research Institute of Industrial Catalysis, East China University of Science and Technology, Shanghai, 200237, PR China

^b School of Material Science and Engineering, Shanghai Jiao Tong University, Shanghai, 200240, PR China

ARTICLE INFO

ABSTRACT

Keywords:
Chlorobenzene
1,2-Dichlorobenzene
Ceria
Tungsten
Catalytic combustion

WO_x/CeO_2 catalysts prepared by wet impregnation with $(\text{NH}_4)_6\text{H}_2\text{W}_{12}\text{O}_{40}$ and $(\text{COOH})_2$ aqueous solution were used in the catalytic combustion of chlorobenzene (CB) and 1,2-dichloro- benzene (1,2-DCB). Characterization by XRD, N_2 isothermal adsorption and desorption, Raman, XPS, H_2 -TPR, O_2 -TPD and NH_3 -TPD shows that CeO_2 exists as a form of face-centered cubic fluorite structure, while WO_x is identified as the forms of monoxo and dioxo monotungstate, polytungstate and nano-particle, depending on W content. $\text{W}-\text{O}-\text{Ce}$ is formed as a result of interaction between WO_x and CeO_2 , which increases oxygen vacancy and promotes the reducibility and acidity of WO_x/CeO_2 catalysts. In CB or 1,2-DCB oxidation, WO_x/CeO_2 catalysts with monotungstate WO_x present excellent stable activity with TOF at 250 °C based on $\text{W}-\text{O}-\text{Ce}$ in a range of $4.7\text{--}7.2 \times 10^{-4} \text{ s}^{-1}$. 90% conversion is obtained below 350 °C, at which chlorination is almost completely inhibited. The activity in feed containing 5% H_2O or 5% CO_2 is depending on their effects on the availability of surface oxygen. *In situ* FT-IR shows that the adsorbed CB species can be oxidized by surface lattice oxygen into phenolate, carboxylates and carbonate, while the formation of acetaldehyde on Brønsted acid sites is promoted by gas oxygen. Partial oxidation products are oxidized to CO_2 by surface oxygen.

1. Introduction

Polychlorinated dibenzo-*p*-dioxins and dibenzofurans (PCDDs and PCDFs) are among the most notorious environmental pollutants [1], due to their potential toxicity as carcinogens and teratogens, bioaccumulation in animals, and long-term persistence in the environment. Among various available catalytic purification methods, the catalytic oxidation is a promising technology for the removal of dioxins in waste gases, due to its low reaction temperature, low consumption of energy and high effectiveness. As the most representative chlorinated aromatic compound with simple structure, chlorobenzene (CB) or 1,2-dichlorobenzene (1,2-DCB) is often employed as the model reagent of PCDDs and PCDFs to predict the catalytic performance of dioxin on various catalysts.

In the past decades, more efforts have been devoted to transition metal oxide catalysts in the studies of catalytic combustion of CB and 1,2-DCB, including Mn [2], Fe [3], Co [4], V [5], Cr [6], Ce [7] oxides, of which CeO_2 has attracted great attention due to its remarkable redox properties and high ability for dissociating C-Cl bonds. However, CeO_2 's deactivation due to strong adsorption of Cl species produced during

CVOCs decomposition [8], high activity for chlorination [9] and low resistance to water [8,9] limited the use in industrial applications. It was found that Cl tended to be adsorbed on oxygen vacancy of CeO_2 [10]. The incorporation of transition metals, such as V and Ti, into CeO_2 could increase and modify chemical environment of oxygen vacancy [9,11]. Another promotion pathway of Cl removal was to increase Brønsted acid, which was favorable for the formation of HCl [12]. Zhou et al introduced Brønsted acid sites into Ce-based catalysts using USY acidic zeolite support and found that the removal of Cl species in CVOCs oxidation was related to Brønsted acidity [12].

As recently reported, the addition of WO_3 into CeO_2 could significantly increased oxygen vacancy on CeO_2 contacted by WO_3 cluster through the increase in reduced ceria [13]. *In situ* UV-vis spectra of WO_3-CeO_2 suggested the increase in the redox performance of CeO_2 species due to $\text{O}_{2p} \rightarrow \text{Ce}_{4f}$ ligand-to-metal charge transfer in interface between WO_3 and CeO_2 [14]. Quick transfer of gaseous oxygen into lattice oxygen occurred in NH_3 -SCR reaction over WO_3-CeO_2 catalysts at low temperatures [15]. Additionally, Brønsted acid sites ($\text{W}-\text{OH}$ resulted from $\text{Ce}_2(\text{WO}_4)_3$ [16]) and Lewis acid sites (W^{6+} and $\text{Ce}^{3+}/\text{Ce}^{4+}$) could be controlled by changing the temperature of calcinations

* Corresponding author.

E-mail address: wangxy@ecust.edu.cn (X. Wang).

[17]. A synergism of acidity and redox was observed over $\text{CeO}_2\text{-WO}_3$ catalysts in $\text{NH}_3\text{-SCR}$ [18]. Similarly, highly active species formed at WO_x -modified interface between PdO_x and TiO_2 particles was responsible for the enhanced catalytic activity of total oxidation of propane over $\text{Pd}_{0.8}\text{/W}_{0.2}\text{/TiO}_2$ catalysts [19]. As known, the commercial $\text{VO}_x\text{/TiO}_2$ catalysts were highly effective for the oxidation of chlorinated aromatics. W-Cl bond possesses lower strength than the V-Cl bond [20]. It is possible for $\text{WO}_x\text{/CeO}_2$ catalysts that WO_x can weaken the strength of Cl adsorption on oxygen vacancy of CeO_2 . Thus, there may be an opportunity to develop $\text{WO}_x\text{/CeO}_2$ catalysts with high catalytic performance for oxidation of chlorinated aromatics. In this work, $\text{WO}_x\text{/CeO}_2$ catalysts with W loading in a range of 0.76–12 wt% were prepared by wet impregnation and investigated in combustive oxidation of CB and DCB. The relation of surface structure and performance to the activity, selectivity and stability for oxidation was studied.

2. Experimental

2.1. Catalyst preparation

$\text{Ce}(\text{NO}_3)_3\cdot 6\text{H}_2\text{O}$ was employed as the precursor to synthesize pure CeO_2 by using hydrothermal method. $\text{Ce}(\text{NO}_3)_3\cdot 6\text{H}_2\text{O}$ (10 g) and urea (3 g) were dissolved in deionized water (40 mL) followed by stirring for 30 min at room temperature. The obtained solution was placed into a 100 mL autoclave made of teflon-lined stainless steel and then heated up to 140 °C which was maintained for 300 min. When cooled down to room temperature naturally, the precipitate was washed with 2 L deionized water, dried at 110 °C overnight, and finally calcined at 450 °C in air for 120 min.

A series of $\text{WO}_x\text{/CeO}_2$ catalysts with W loading in a range of 0.76–12.00 wt.% were prepared by wet impregnation. The above obtained CeO_2 was impregnated with a given amount of aqueous solution containing $(\text{NH}_4)_6\text{H}_2\text{W}_{12}\text{O}_{40}$ and $(\text{COOH})_2$ with molar ratio of 1:1, then dried and finally calcined according to the same method as that for pure CeO_2 . The obtained catalyst is denoted as yW, where y is W density, referring to the number of W atom per square nanometer. For example, 1.0 W sample possesses W density of 1.0 W atom/ nm^2 . The W density of $\text{WO}_x\text{/CeO}_2$ samples is in a range of 0.24–6.5 W atom/ nm^2 .

2.2. Catalyst characterization

The characterizations by nitrogen adsorption and desorption isotherms, X-ray diffraction patterns (XRD), Raman, X-ray photoelectron spectroscopy (XPS), NH_3 temperature programmed desorption ($\text{NH}_3\text{-TPD}$), temperature programmed surface reaction (TPSR) measurement were similar to the previously reported work [11]. Hydrogen temperature-programmed reduction ($\text{H}_2\text{-TPR}$) tests were performed by using a conventional apparatus equipped with TCD. Prior to the test, sample (100 mg) was pre-treated at 400 °C with He flow (30 mL/min) for 60 min and then cooled to 50 °C. $\text{H}_2\text{-TPR}$ was recorded from 50 to 750 °C in 5% $\text{H}_2\text{/He}$ flow (30 mL/min) at a heating rate of 10 °C/min. H_2 consumption was quantitatively calculated according to areas under reduction peaks with calibration against a known amount of standard CuO sample. Oxygen temperature-programmed desorption ($\text{O}_2\text{-TPD}$) tests were performed by Micromeritics 2920 apparatus equipped with a quadrupole mass (Q-MASS) detector. Sample (100 mg) was pretreated at 400 °C with He flow (30 mL/min) for 60 min, and subsequently treated by 5% $\text{O}_2\text{/He}$ (30 mL) for 120 min, then cooled down to 50 °C. After being purged with He flow (30 mL/min), the sample was heated from 50 to 700 °C in He flow (30 mL/min) at a heating rate of 10 °C/min.

2.3. Catalytic activity measurements

Catalytic oxidation performances of as-prepared $\text{WO}_x\text{/CeO}_2$ catalysts were investigated with a quartz reactor ($D = 4\text{ mm}$). In a standard

test, 200 mg grain catalyst (40–60 mesh) was packed in the reactor bed. The feed was set at 100 ml/min, composed of 0.1% CB or DCB and 10% O_2 with N_2 balance, and gas hour space velocity (GHSV) was 60,000 h^{-1} . The range of reaction temperature was set at 90–450 °C. Organic compounds in effluents were determined on-line using GC (GC9790, FULI) equipped with a flame ionization detector and a flap-30 m × 0.32 mm × 0.50 μm capillary column, Considering the change in feed volume to be negligible, the conversion was estimated by the difference between initial and final CB or DCB concentration divided by initial CB or DCB concentration. Cl_2 was detected by chemical titration of a 0.0125 N NaOH solution through which effluent stream bubbles with ferrous ammonium sulphate using *N,N*-diethyl-p-phenylene-diamine as an indicator.

2.4. In situ FTIR

Nicolet 6700 FTIR equipped with liquid nitrogen cooled mercury-cadmium-telluride detector was used to operate *in situ* diffuse reflectance infrared Fourier transform spectroscopy (DRIFTS) experiments. DRIFTS cell (Harrick, HVC-DRP) fitted with CaF_2 window was used as the reaction chamber that allowed samples to be heated to 650 °C, and the spectra were recorded within a frequency range of 4000–1000 cm^{-1} at the resolution of 4 cm^{-1} and 64 scans. 80 mg grain catalyst (40–60 mesh) was packed in DRIFTS cell. For CB adsorption spectra, the samples were pretreated at 450 °C by flowing Ar for 120 min with subsequent exposure to 1000 ppm CB/Ar feed to saturation at different temperature, and then to Ar for 30 min. For CB oxidation spectra, the atmosphere used for treating catalysts was 10% O_2 /Ar flow, and the feed was (1000 ppm CB + 10% O_2)/Ar.

3. Results and discussions

3.1. Catalyst characterization

3.1.1. Physical properties

The W content of $\text{WO}_x\text{/CeO}_2$ samples is determined by ICP-AES to be in a range of 0.76–12 wt% with W density of 0.24–6.5 W atom/ nm^2 . N_2 adsorption and desorption isotherms (Fig. S1) show that $\text{WO}_x\text{/CeO}_2$ samples have regularly stacking tubular pores with the pore size distributions of 3.5–5.1 nm calculated from the desorption isotherm branch based on BJH model (Table 1). For the samples with 2.4 W atom/ nm^2 or higher, pore volume decreases to a slight extent. Correspondingly, the surface area determined by BET method based on nitrogen adsorption isotherm decreases from 100 to 107 to 61 m^2/g (Table 1), probably due to excess coverage of WO_x . On XRD patterns (Fig. 1), there appear the diffraction peaks at 28.6, 33.3, 47.5, 56.5 and 59.2°, ascribed to <111>, <200>, <220>, <311> and <

Table 1
Structure and physical parameters of $\text{WO}_x\text{/CeO}_2$ samples.

Sample	$S_{\text{BET}}^{\text{a}}$ $/ \text{m}^2/\text{g}$	$V_{\text{pore}} / \text{cm}^3/\text{g}$	$D_{\text{pore}} / \text{nm}$	W Loading ^b / wt.%	W density ^c / W atom/ nm^2	R ^d / nm	L ^e / nm
CeO_2	107	0.093	3.5	—	—	13.4	0.5409
0.24 W	104	0.096	3.7	0.76	0.24	13.9	0.5416
0.5 W	100	0.093	3.6	1.6	0.5	13.6	0.5413
1.0 W	100	0.090	4.0	3.2	1.0	13.5	0.5405
2.4 W	85	0.085	4.0	6.2	2.4	13.2	0.5409
3.4 W	72	0.078	4.3	7.5	3.4	13.1	0.5413
6.5 W	61	0.077	5.1	12.0	6.5	13.3	0.5405

^a Surface area determined from N_2 adsorption isotherm.

^b Determined by ICP-AES.

^c Calculated according to S_{BET} and W content measured by ICP.

^d Crystallite size estimated by the Scherrer equation, applied to the (111) plane of fluorite CeO_2 .

^e Lattice parameter.

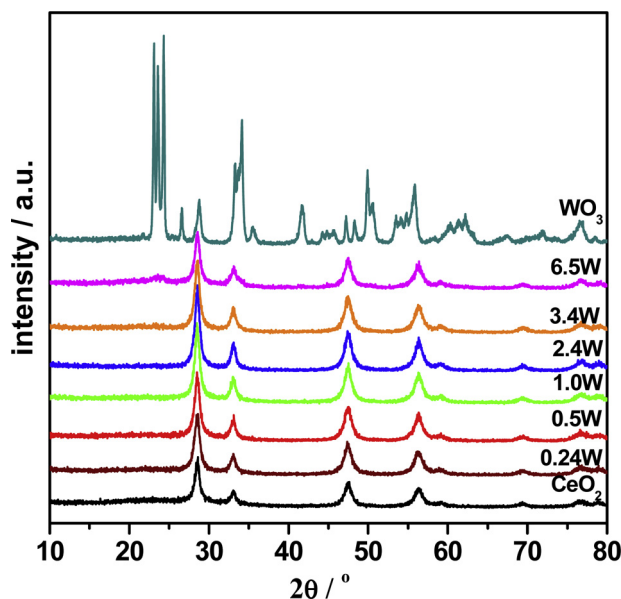


Fig. 1. XRD patterns of WO_x/CeO_2 catalysts with various W loadings.

$400 >$ planes of cubic fluorite CeO_2 , respectively (PDF# 34-0394). The diffraction peak at 23.7°, ascribed to crystal WO_3 (PDF# 20-1324), is observed only for the samples with 3.4 W atom/ nm^2 or higher. For the samples with low W density, W species should be highly dispersed on CeO_2 surface. Considering the fact that the ratio of W^{6+} (0.62 Å) species is smaller than that of Ce^{4+} species (0.92 Å), it seems possible that W^{6+} species could enter into the lattice of CeO_2 to form W-O-Ce solid solution. However, the lattice parameter of the cubic fluorite phase of CeO_2 for WO_x/CeO_2 catalysts is estimated to be 0.5411 ± 0.0006 nm (Table 1), almost similar to that for pure CeO_2 . Because there is a large difference in ionic radii between W^{6+} and Ce^{4+} , the replacement of Ce^{4+} by W^{6+} to form a solid solution is unexpected. A more likely explanation is that WO_3 moieties are directly bonded to the CeO_2 surface as amorphous structures by W-O-Ce linkages [18].

Raman spectra (Fig. 2) of CeO_2 are dominated by a strong F2g mode

of fluorite phase at 456 cm^{-1} , companying weak 2TA, D and 2LO mode at 265, 598, and 1175 cm^{-1} , respectively [21]. The ν_{F2g} band is resulted from oxygen lattice vibrations, sensitive to crystalline symmetry [21]. It becomes quickly weak with W loading, due to the lattice distortion of CeO_2 . DFT calculation showed that Ce-O bond length became large near a W-atom placed on CeO_2 (111) surfaces, which could weaken the Ce-O bond [22]. Additionally, the band at 880 cm^{-1} ascribed to W-O-Ce species is observed, indicating that main part of W atoms take the place of surface Ce atoms, forming W-O-Ce linkages [18]. For VO_x/CeO_2 , V-O-Ce appeared at 832 cm^{-1} [11]. The band at 598 cm^{-1} is ascribed to oxygen vacancy and the ratio of I_{598}/I_{460} becomes large with W content. Theoretical calculations indicated that the formation of oxygen vacancy preferentially occurred at the interfaces between CeO_2 and doped metal oxide crystallites [23]. For the samples with WO_x domain, the interactions between aqueous polytungstate oligomers and CeO_2 or the formation of Ce-containing heteropolytungstate intact or lacunary clusters were favorable for the formation of oxygen vacancy in the interface [24]. As reported, the band at 833 cm^{-1} could be assigned to peroxy-like species at oxygen vacancies in WO_3/CeO_2 [25]. The peroxy-like species could be observed on CeO_2 surfaces with treatment by reductive gas following exposure to O_2 . In this test, almost no band at 833 cm^{-1} on the samples dehydrated at 300 °C appears, probably due to desorption of reversibly adsorbed peroxy-like species. Additionally, the band at 1175 cm^{-1} , ascribed to superoxo (O_2^-) species, is observed [25]. And the ratio of I_{1175}/I_{460} decreases with W content (Table 2), indicating that superoxo (O_2^-) species comes mainly from the bare CeO_2 .

The structural information about WO_x species is obtained also in Fig. 2. The band at 977 cm^{-1} is ascribed to the terminal W=O bond stretching modes of monotungstate monoxo WO_5 ($\text{O} = \text{W}(\text{O}-\text{Ce})_4$), where one W atom contacts with four Ce atoms to form four W-O-Ce. For the samples with 1.0 W atom/ nm^2 or higher, there appears a new band at about 958 cm^{-1} , which can be assigned another kind of terminal W=O bond of monotungstate, dioxo WO_4 ($(\text{O} =)_2\text{W}(\text{O}-\text{Ce})_2$), corresponding two W-O-Ce. For dehydrated W_3Ce or W_1Ce catalyst prepared by co-precipitation, the dioxo structure of W=O was detected only at 929 cm^{-1} [18]. Monoxo W=O was observed at 1001 cm^{-1} for dehydrated 0.5 W atom/ nm^2 WO_3/SiO_2 , while for dehydrated 0.5 W atom/ nm^2 $\text{WO}_3/\text{Al}_2\text{O}_3$, the bands of monoxo and dioxo W=O appeared at 1015 and 985 cm^{-1} [26]. The difference in frequency should be

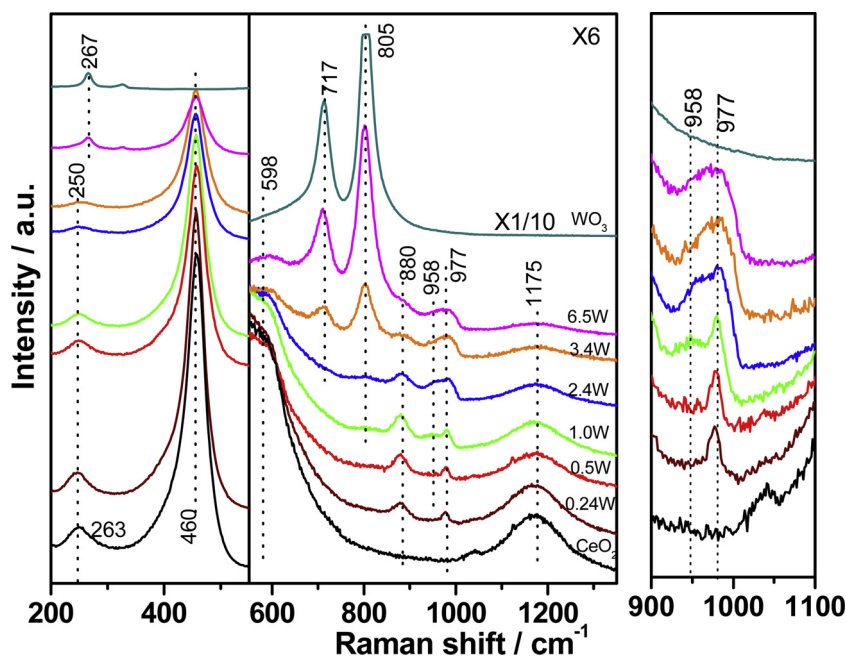


Fig. 2. The dehydrated Raman spectra of WO_x/CeO_2 samples.

Table 2The Raman results and the acidity of WO_x/CeO_2 samples.

Sample	$I_{598}/I_{460}^{\text{a}}$	W-O-W (717, 805 cm^{-1})	W-O-Ce (880 cm^{-1})	$I_{1175}/I_{460}^{\text{b}}$	monoxo WO_5 (977 cm^{-1})	dioxo WO_4 (957 cm^{-1})	Acid / umol/m ²	
							weak	strong
CeO_2	0.0146	—	—	0.064	—	—	0.54	0.77
0.24 W	0.0152	X	✓	0.063	✓	X	0.56	1.11
0.5 W	0.0157	X	✓	0.059	✓	X	0.56	1.20
1.0 W	0.0161	X	✓	0.057	✓	✓	0.60	1.74
2.4 W	0.018	✓	✓	0.056	✓	✓	0.68	1.85
3.4 W	0.0177	✓	✓	0.055	✓	✓	0.79	2.06
6.5 W	0.0169	✓	✓	0.053	✓	✓	0.98	1.35

^a The ratio of band intensity (598 to 460 cm^{-1}).^b The ratio of band intensity (1175 to 460 cm^{-1}).

related to the interaction between WO_3 and different matrix. For 3.4 W, the band at 958 cm^{-1} becomes weak, and the band in a range of 920–1000 cm^{-1} , broad, indicating that polytungstate W–O–W forms on CeO_2 , which is confirmed by the bands at 267, 717 and 805 cm^{-1} ascribed to W–O–W vibration mode [18], which is consistent with the reflection from WO_3 crystal on XRD pattern. This result could suggest excess WO_x over a monolayer coverage on CeO_2 . That is to say, a monolayer coverage of WO_x should be closed to 3.4 atom/nm². On Al_2O_3 , ZrO_2 , TiO_2 and Nb_2O_5 , a monolayer coverage of WO_x corresponded to 4–5 W atom/nm² [26–28]. For pure WO_3 , the bands corresponding to both monotungstate and polytungstate species disappear.

3.1.2. Chemical states and reduction behavior of catalysts

XPS spectra of W 4f, O 1s, and Ce 3d for WO_x/CeO_2 samples are shown in Fig. 3. For W 4f, the binding energies (BE) of W 4f_{5/2} and 4f_{7/2} are 37.5 and 35.3 eV, respectively, suggesting that W exists as W⁶⁺ (Fig. 3A) [29]. W 4f peaks overlap with Ce 5s peaks, especially for the samples with low W content, which is similar to the overlap of W 4f peaks with Ti 3s peaks [30]. On O 1s spectra (Fig. 3B), two states of oxygen species are identified with a deconvolution method. BE of lattice oxygen (O_{latt}) is 529.4–529.9 eV, and one of surface-adsorbed oxygen (O_{sur}), 531.0–531.3 eV. The samples with monotungstate WO_x present similar BE of O_{latt} (529.3–529.5 eV), which is similar to that of CeO_2 (529.3 eV). Raising W content, BE increases gradually and finally up to 529.9 eV for 6.5 W, indicating that O 2p → Ce 4f ligand-to-metal charge transfer bands in the interface between CeO_2 and WO_x species can be promoted with the formation of W–O–W [31]. The ratio of $\text{O}_{\text{sur}}/\text{O}_{\text{total}}$ (Table 3) remains constant at W density below 1.0 W atom/

nm², and after that remarkably reduces, due to a significant decrease in the exposed CeO_2 . As known, surface-adsorbed oxygen (O_{sur}) species such as active oxygen O_2^- , O^- and hydroxyl group exist on CeO_2 . FT-IR spectra confirm that hydroxyl group at 3708–3712 cm^{-1} from CeO_2 becomes weak with W loading (not shown). Here, O_{sur} should not include O_2^{2-} species which is removed due to desorption under XPS ultra-high vacuum conditions (O_2 -TPD tests in Fig. 4B confirm significant desorption of reversibly adsorbed O_2^{2-} species at low temperature). On Ce 3d spectra, the identified peaks with deconvolution method can be caused by the pairs of spin orbit doublets (Fig. 3C). Ce^{4+} contributes to six peaks denoted as v, v'', v''' u, u'', u''' and Ce^{3+} , to peaks as v', u' [32]. Ce^{3+} species increases with W loading, which is related to the promotion of WO_x to the formation of reduced Ce centers near the interfaces [15].

H_2 -TPR profiles for WO_x/CeO_2 samples are shown in Fig. 4A. Before the tests, all samples were pretreated in He at 400 °C, and thus the adsorbed oxygen and surface oxygen should be ignored (see O_2 -TPD). A broad reduction peak appears at 300–580 °C with similar peak shape. For pure CeO_2 , there occurs mainly the reduction of surface Ce^{4+} to Ce^{3+} , and a shoulder peak at 348 °C is related to the reduction of Ce^{4+} on highly dispersed CeO_2 . With W loading, this peak disappears quickly, indicating that WO_x interacts preferentially with defective sites on CeO_2 , as shown in the cases of $\text{ZrO}_2\text{-CeO}_2$ [33] and $\text{CuO}\text{-CeO}_2$ [34]. On high temperature side, the profile shifts to high temperature with the increase in H_2 consumption. The theoretical H_2 consumption is estimated according both to H_2 consumption per square meter of CeO_2 (normalized by Ce^{4+} composition obtained from XPS analyses) and to that needed for reduction of the loaded W⁶⁺ to W⁴⁺ (Table S1). As

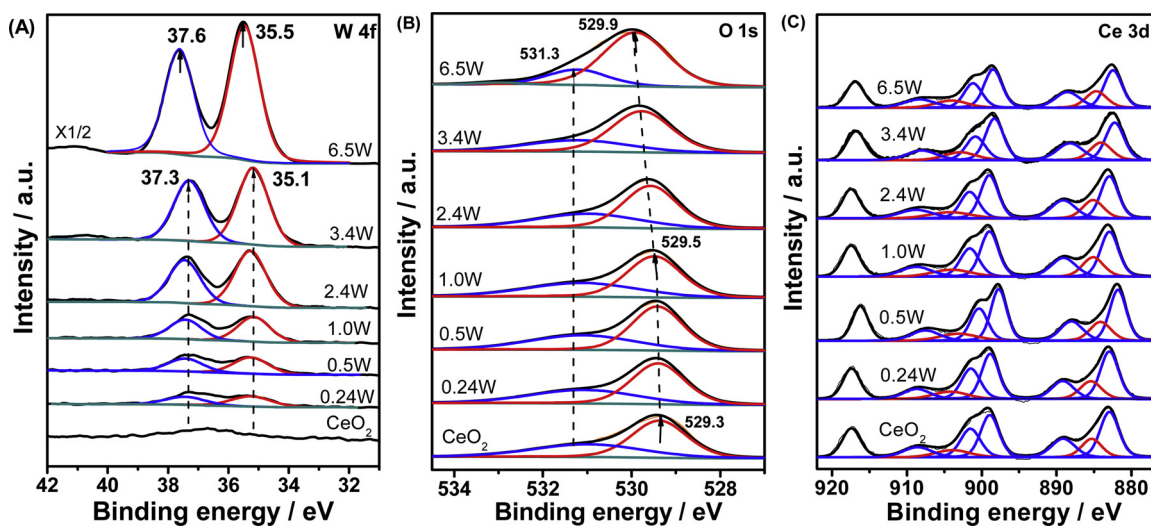
Fig. 3. XPS spectra of W4f (A), O 1s (B) and Ce 3d (C) for WO_x/CeO_2 catalysts.

Table 3 H_2 consumption, O_2 desorption and XPS data of WO_x/CeO_2 samples.

Sample	H_2 cons. ^a / mmol. g ⁻¹	H_2 cons. ^b / mmol. g ⁻¹	$O_{\text{sur}}/O_{\text{total}}$ ^c		Ce^{3+}/Ce ^c		Cl /at% ^c	O_2 desorption /a.u. ^d		
			fresh	used	fresh	used		$P_{250}(O_2^{2-})$	$P_{350}(O_2^{-})$	$P_{450}(O^-)$
CeO ₂	1.12	—	0.41	0.22	0.15	0.13	4.8	—	1.58	2.21
0.24 W	1.17	1.09	0.40	0.31	0.16	0.14	4.5	—	0.91	2.25
0.5 W	1.21	1.10	0.41	0.33	0.16	0.157	4.5	—	0.91	1.38
1.0 W	1.28	1.18	0.41	0.34	0.16	0.16	4.1	—	0.88	0.85
2.4 W	1.25	1.19	0.38	0.32	0.16	0.16	3.1	0.45	0.54	0.41
3.4 W	1.51	1.13	0.32	0.30	0.17	0.15	2.9	0.76	0.49	0.46
6.5 W	1.69	1.26	0.21	0.18	0.17	0.14	1.9	1.57	0.44	0.51

^a Experimental H_2 consumption.^b Theoretical H_2 consumption (SI), estimated based on an assumption that the contribution is mainly from the reduction of both surface Ce^{4+} and W^{6+} to W^{4+} of WO_x .^c The values estimated with XPS results.^d The area of desorption obtained at 250, 350 and 450 °C on O_2 -TPD profiles normalized by the surface area.

shown in Table 3, the experimental H_2 consumptions are higher than the calculated values, suggesting that at least, a part of WO_x species or/and a part of bulk Ce^{4+} species are reduced. In fact, pure WO_3 cannot be reduced until 600 °C (Fig. S2). Obviously, the reduction of WO_x and CeO_2 is promoted by the formation of W-O-Ce. For WO_x/CeO_2 catalysts, because either the formation of H^{n+} species or by the removal of H_2O to form O-vacancies, d-d transitions in W^{5+} centers become facile, which is favorable for the reduction of W^{6+} . This feature becomes more intense with increasing H_2 treatment temperatures. And such W^{6+} reduction processes become more facile as domains become larger, because of more effective electron delocalization during reduction. M. Iwasaki et al observed the increased in the number of Ce^{3+} and W^{5+} centers using UV visible spectroscopy on WO_3/CeO_2 (5.3 W nm²) during H_2 treatment at 100–350 °C [14].

O_2 -TPD tests of WO_x/CeO_2 samples were carried out to determine the mobility of oxygen species. Before the test, the sample was pretreated with He flow at 400 °C. Generally, the temperature order of O_2 desorption is physically adsorbed oxygen $O_2 <$ reversibly and chemically adsorbed oxygen $O_2^{2-} <$ irreversibly and chemically adsorbed oxygen $O_2^- <$ surface O- species < lattice O^{2-} species (500 °C for weak surface lattice oxygen and for bulk lattice oxygen 750 °C or higher) [35]. As the superoxide species (O_2^-) are formed immediately after O_2 introducing onto CeO_2 and successively converted into O_2^{2-} , O_- , and finally into O^{2-} by accepting more electrons from the surface. O_2^- species are formed when O_2 gains two electrons, which weaken the O–O bond strength markedly so that the species are different from O_2^- . Enrique Iglesia found the presence of O_2^{2-} species only on CeO_2 exposed to O_2 after treated by H_2 [14]. In this work, for CeO_2 exposed to O_2 after treated by He, there appear three peaks with maxima at 350, 450 and 580 °C (Fig. 4B), which should be ascribed to the desorption of surface oxygen O_2^- and O_- , and surface lattice oxygen O^{2-} , respectively, of which O_2^- (super oxygen) as Raman active species is confirmed at 1175 cm⁻¹. With W loading, the desorption of different oxygen species becomes weak, and the corresponding density of O_2^- and O_- decreases (Table 3), indicating that the contribution to the surface oxygen species are mainly from CeO_2 . However, 6.5 W presents similar density of O_2^- and O_- to 2.4 W and 3.4 W, which is related probably to that surface oxygen in oxygen vacancy can be promoted by WO_x domains to some extent. It is interesting to find that for 2.4 W, 3.4 W and 6.5 W, there appears a desorption peak with maximum at 250 °C overlapping on the peak of O_2^- and the peak area becomes large with W loading. UV-vis spectra at 200–350 °C for WO_x/CeO_2 catalyst with 5.2 W atom /nm² pretreated with He before exposure to O_2 (g) showed that there existed a large amount of oxygen chemisorbed reversibly on oxygen vacancies as a form of peroxy-like O_2^{2-} [14]. In this experiment, WO_3 domains on CeO_2 allow the formation of reduced Ce centers in He (at 400 °C) near their interfaces via W-O-Ce interaction, leading to the formation of O_2^{2-} species upon contact with O_2 . This result is consistent with that

obtained from UV-vis features of WO_x/CeO_2 [14].

3.1.3. Acidity

NH_3 -TPD profiles of the samples shown in Fig. S3A are divided into two sections of 100–300 and 300–600 °C, corresponding to ammonia desorbed from weak and moderate-strong acidic sites (Fig. S3C). The acid amounts of samples are estimated according to the relationship of peak area with acidity (Table 2). CeO_2 presents a total acid density of 1.3 umol/m² with weak/strong acid ratio of 0.70. With W loading, weak acid almost linearly and slowly increases, while strong acid increases at first quickly from 0.77 umol/m² for CeO_2 to 1.74 umol/m² at 1.0 W atom/nm², then slowly to 1.85 umol/m² at 2.4 W atom/nm², and finally decreases down to 1.35 umol/m² at 6.5 W atom/nm². On Py-FT-IR spectra (Fig. S3B) of the samples evacuated at 200 °C, the band at 1440 cm⁻¹, ascribed to Lewis acid, is observed, whose strongest intensity is obtained at 2.4 W atom/nm². Lewis acidic sites are composed of Ce^{3+}/Ce^{4+} and W^{6+} ions. Highly unsaturated W^{6+} as strong Lewis acid site can be promoted by monotungstate WO_x on CeO_2 [17]. Moreover, there appears the band at 1550 cm⁻¹ only for WO_x/CeO_2 samples, suggesting the presence of Brønsted acid. As known, Brønsted acid sites are related only to W–OH sites [31] arising from partially hydrated tungsten species, such as $W=O$, $W-O-W$, and $Ce-O-W$ [36]. It should be noted that 1.0 W and 2.4 W, which possess most monotungstate dioxo WO_4 , present the strongest band at 1550 cm⁻¹. In fact, phosphotungstic heteropoly acids present strong Brønsted acids through the combination of $4W=O$ with $1/2H_2O$ to form H^+ . As expected, the increase in monotungstate dioxo WO_4 effectively promotes hydration, which, in turn, increases Brønsted acidity.

3.2. Activity

WO_x/CeO_2 catalysts were evaluated kinetically for the activity for CB and DCB oxidation as functions of temperature (Fig. 5). CeO_2 shows a significant activity and the conversion reaches 90% at 440 °C. With W loading, the conversion curves shift gradually to low temperature. 2.4 W presents the highest apparent activity, on which the temperature needed for 90% conversion (T_{90}) of CB and DCB is 339 °C. Fig. 6(A) shows that T_{90} for the catalysts with monotungstate WO_x is lower than the catalysts with polytungstate WO_x . 3.4 W and 6.5 W present low activity at high temperature, T_{90} for CB rise up to 388 and 484 °C, and for DCB, 388 and 536 °C. On the other hand, for benzene (B) without Cl, T_{90} over CeO_2 , 0.24 W, 0.5 W and 1.0 W decreases to a large extent. The negative effect of high W loading on the activity for B oxidation is observed. The difference in activity between CB or DCB and B oxidation becomes small with the increases in W loading, indicating that Cl removal should be a slow process. The incorporation of W into CeO_2 can promote Cl removal from catalyst surface, as reported for chlorinated aromatics oxidation on Ti, Ru and Mn doped CeO_2 catalysts [9,32,37].

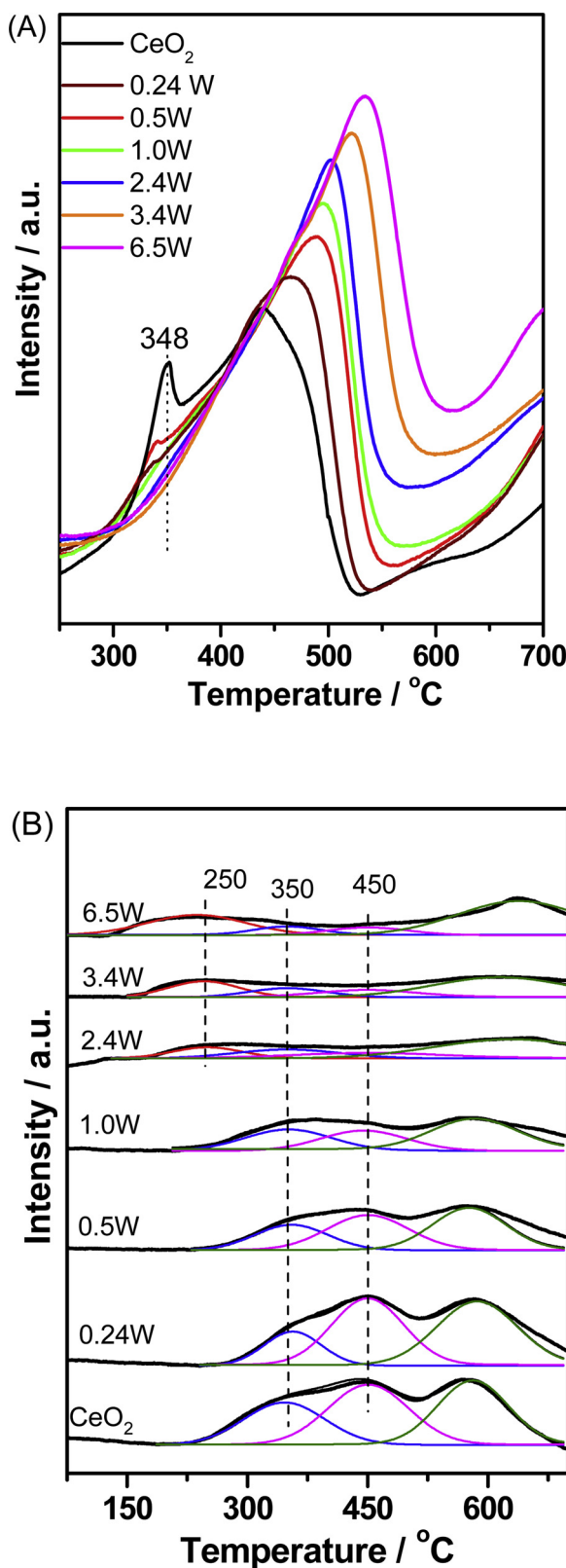


Fig. 4. H_2 -TPR (A) and O_2 -TPD (B) profiles of WO_x/CeO_2 samples.

Considering the difference in the surface area of WO_x/CeO_2 catalysts with various W loadings, the rate at 250 $^{\circ}\text{C}$ is estimated according to the mole number of CB and 1,2-DCB transformed within unit area and unit time (Table 4). Both rates are promoted with the increase in W loading and reach the highest for 3.4 W, whose coverage of WO_x is near one-

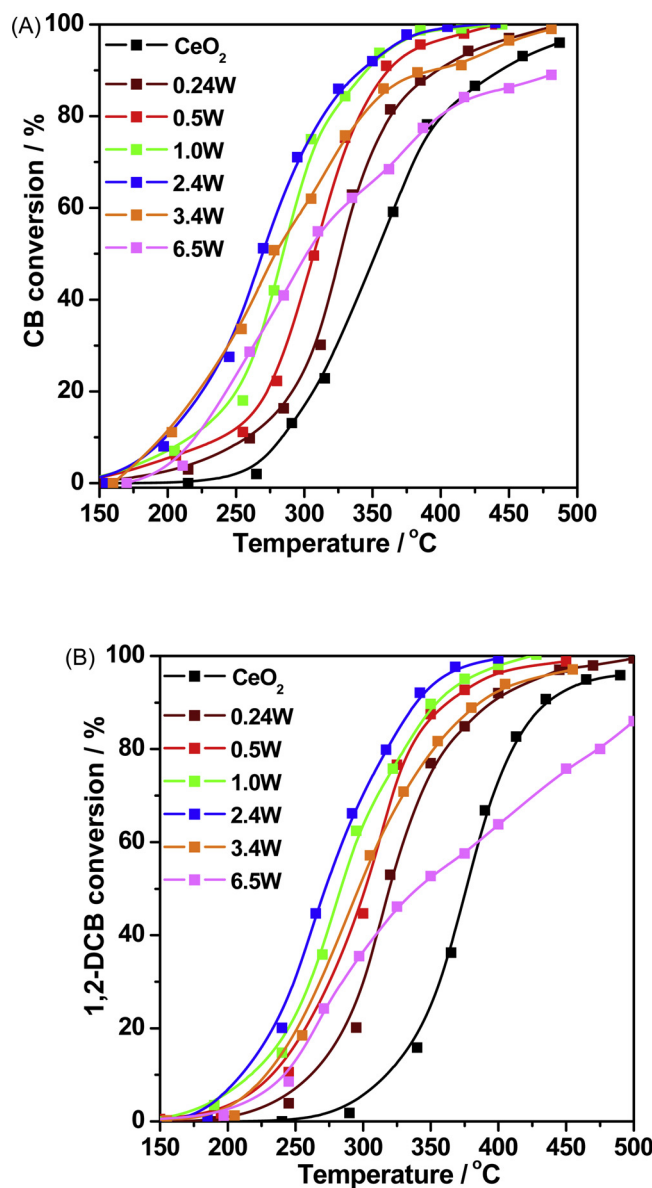


Fig. 5. Conversion curves for CB (A) and DCB (B) oxidation over WO_x/CeO_2 catalysts; gas compositions: 1000 ppm CB, 10% O_2 and N_2 balance; GHSV: 60,000 h^{-1} ; catalyst amount: 200 mg.

layer. Combining the fact that pure WO_3 and CeO_2 are not active at 250 $^{\circ}\text{C}$, it can be considered that the reaction occurs mainly on the active sites related to W-O-Ce, which promotes the removal of Cl. Indeed, the rate for CB oxidation is inversely proportional to Cl adsorption on the used catalysts (XPS data) (Fig. S4). The formation of W-O-Ce in the interface between WO_x and CeO_2 promotes both strong Brønsted and Lewis acidity (Fig. S3). Zhou found that the removal of Cl species in CVOCs oxidation on zeolite catalysts was related to Brønsted acidity [12]. Our previous first-principles density functional theory calculations showed that Cl produced during the decomposition of CVOCs preferably located at the oxygen vacancy of CeO_2 [10], which led to the deactivation of active sites involving in oxygen adsorption. The increase in BE of lattice oxygen due to $\text{O } 2\text{p} \rightarrow \text{Ce } 4\text{f}$ ligand-to-metal charge transfer bands may result in the decrease in strength of Cl adsorption on CeO_2 species (Table 4). As known, the commercial VO_x/TiO_2 catalysts were highly effective for the oxidation of chlorinated aromatics. Moreover, the W-Cl bond possesses lower strength than the V-Cl bond [20], leading to high availability of W^{6+} Lewis acid sites for CB or 1,2-DCB adsorption.

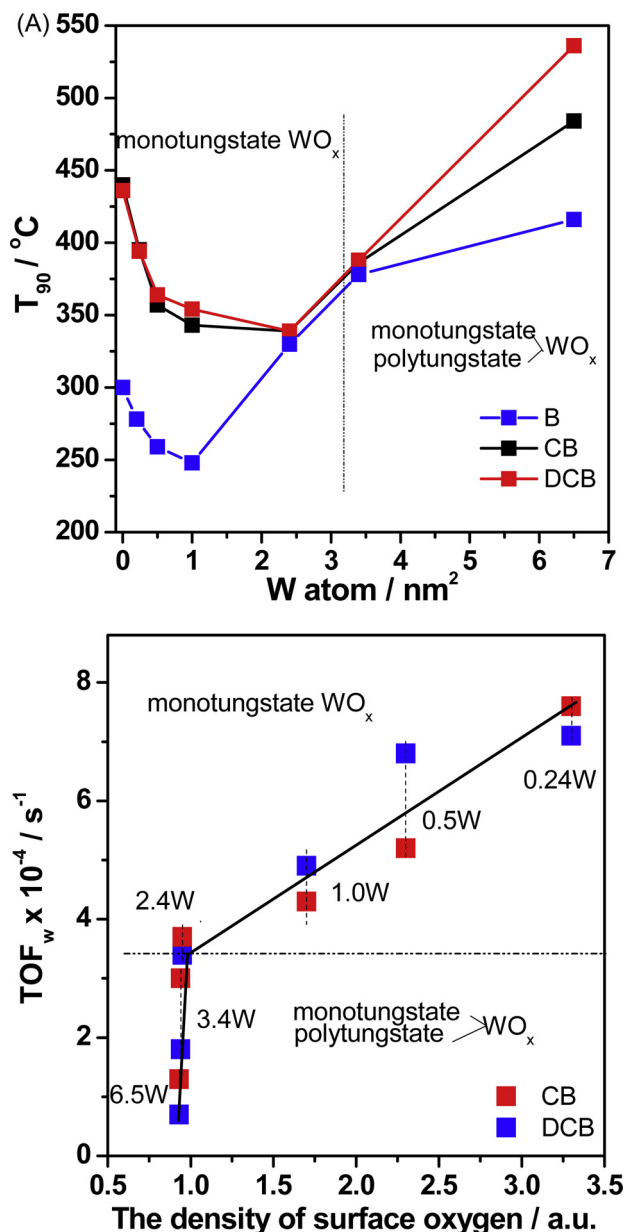


Fig. 6. T_{90} for B, CB and 1,2-DCB combustion over WO_x/CeO_2 catalysts (A); TOF_w for CB and DCB oxidation at 250 °C over WO_x/CeO_2 catalysts vs surface oxygen estimated from O_2 desorption peaks with maxima at 350 °C and 450 °C in O_2 -TPD profiles(B); gas compositions; 1000 ppm reactant, 10% O_2 and N_2 balance; GHSV: 60,000 h⁻¹; catalyst amount: 200 mg.

Table 4
Activity of WO_x/CeO_2 catalysts for CB, DCB and B combustion.

Sample	CB					DCB					B		
	T_{50} / °C	T_{90} / °C	Rate ₂₅₀ umol/min m ²	$\text{TOF}_w^a \times 10^{-4} \text{ s}^{-1}$	Ea KJ/mol	T_{50} / °C	T_{90} / °C	$\text{TOF}_w \times 10^{-4} \text{ s}^{-1}$	Ea KJ/mol	T_{50} / °C	T_{90} / °C	Ea KJ/mol	
CeO_2	352	440	0.004	—	81.2	377	434	—	81.1	214	300	53.8	
0.24 W	325	395	0.018	7.6(7.2)	52.2	319	400	7.1	68.4	211	278	35.7	
0.5 W	306	357	0.026	5.2(5.9)	46.8	302	367	6.8	61.8	210	259	30.7	
1.0 W	281	343	0.045	4.3(5.6)	42.6	283	347	4.9	52.0	214	248	26.8	
2.4 W	266	339	0.089	3.7(4.7)	50.6	270	346	3.4	60.7	238	330	37.8	
3.4 W	277	389	0.103	3.0(3.7)	51.4	297	388	1.8	67.0	240	378	40.7	
6.5 W	301	484	0.083	1.3(1.4)	67.5	341	536	0.7	70.2	266	416	51.2	

^a The values within brackets are the stable TOF_w obtained in stability test for 50 h.

Because the modification of CeO_2 by other metal oxides was localized [38], TOF_w based on W atom (SI) can be used to investigate the activity of W-O-Ce with different chemical environments. As shown in Fig. 6(B), with the decrease in the density of surface oxygen (the total amount of O_2^- and O^-), the catalysts with monotungstate WO_x presents the slowly decreased TOF_w , indicating that the W-O-Ce around by more surface oxygen is more active. Although 3.4 W and 6.5 W catalysts with polytungstate WO_x (W-O-W structures) possess similar density of surface oxygen to 2.4 W, their TOF_w values decrease quickly due either to the decrease in the number of active W-O-Ce sites based on one W atom or to W-O-Ce's being separated from surface oxygen by W-O-W species or WO_x nano-particles. In fact, WO_x species without contact with CeO_2 almost is not active for CB oxidation, as observed on WO_3 which presents no any reducibility (Fig. S14). Additionally, terminal $\text{W} = \text{O}$ on the other supports such as TiO_2 , Al_2O_3 , SiO_2 is observed to have poor activity for CB oxidation (Fig. S19). Thus, WO_x species formed by excess W loading is negligible for the contribution to activity, and TOF_w drops quickly with the formation of W-O-W species, as observed on 3.4 W and 6.5 W catalysts. If we use the density of total surface oxygen species (normalized by the surface area), it can be found that with the increase in W density from 2.4 to 6.5 W atom/nm^2 , the density of surface oxygen species increases gradually, due to the increase in contribution from the peroxide species to surface oxygen (Table 3), while TOF_w decreases from 3.7 to $1.3 \times 10^{-4} \text{ s}^{-1}$ (Table 4). Therefore, for WO_x/CeO_2 catalysts, the peroxide species almost cannot contribute to activity for CB or DCB oxidation. This phenomenon is really different from the case of NO oxidation over WO_x/CeO_2 catalyst with 5.2 W atom/mn^2 , where peroxy-like O_2^{2-} could be dissociated into active surface oxygen. Decreasing O_2 concentration ($[\text{O}_2]$) from 10% to 0.7% (stoichiometry value for complete oxidation) with keeping CB concentration ([CB]) at 1000 ppm, the activity of 1.0 W decreases to a small extent, while 6.5 W becomes less active (Fig. S5A), and the conversion cannot reach 50% until 460 °C, confirming that the oxygen vacancy contacted with monotungstate WO_x is more favorable for oxygen adsorption and activation than that with polytungstate WO_x . On the other hand, increasing [CB] from 1000 to 3000 ppm at 10% $[\text{O}_2]$, TOF_w of 1.0 W is as three times as that obtained at 1000 ppm [CB] (Fig. S5B), suggesting that the increase in the amount of Cl produced during CB decomposition cannot decrease the availability of O_2^- and O^- species on CeO_2 contacted with WO_x . In other words, the surface oxygen on the interface for the catalysts with monotungstate WO_x is resistant to Cl substitution. XPS results for the used catalysts confirm that the decrease in surface oxygen becomes small gradually with W content (Table 3). For 6.5 W, TOF_w increases by about 0.7 times, indicating that the dependency on [CB] is below first order, that is, there is no enough surface oxygen to meet the need for CB oxidation. Thus, high activity is a synergism between the removal of Cl species and effective oxidation which occurs on the interface between WO_x and CeO_2 .

With the assumption that reactant concentration has not obvious change within 20% conversion, the apparent activation energies (Ea) can be estimated with 95% confidence limits using dependence of the

reaction rate on the reaction temperature (Fig. S6, Table 4). The Ea for CB or 1,2-DCB oxidation is about 81 kJ/mol for CeO₂. CeO₂ was considered as an efficient catalyst for Deacon reaction (HCl + O₂ → Cl₂ + H₂O) at 350–450 °C with Ea of 70–90 kJ/mol, depending on [O₂] [39]. Considering the fact that CeO₂ has a high activity for B oxidation (Ea = 53.8 kJ/mol (Table 4)), it can be considered that the rate-controlling-step for CB or 1,2-DCB oxidation is the removal of Cl species as Cl₂ from the surface of CeO₂. The catalysts with monotungstate WO_x possess the reduced Ea values for CB and 1,2-DCB in a range of 42–52 and 52–68 kJ/mol, respectively, indicating that the increase in interface between CeO₂ and WO_x is favorable for Cl removal. For 6.5 W, the formation of polytungstate or nano-particle WO_x makes Ea increase to some extent. It should be noted that Ea obtained over WO_x/CeO₂ catalysts with various W densities are essentially similar, which indicates that the slow step for reaction is similar, the removal of Cl species from W-O-Ce species. The decrease in TOF_w of the catalysts with polytungstate or nano-particle WO_x can be ascribed either to the decrease in the number of active W-O-Ce sites based on one W atom or to W-O-Ce's being separated from surface oxygen by W-O-W species or WO_x nanoparticles. Additionally, the Ea for B oxidation decreases to 26.8–40.7 kJ/mol for WO_x/CeO₂ catalysts (except for 6.5 W) (Table 4), which should be related to the activation of benzene ring on acid sites which compensates the negative effect of the decrease in surface oxygen. Based on TOF_w values, it can be concluded that the activity order for CB and 1,2-DCB oxidation of WO_x species supported on CeO₂ follows as monotungstate > polytungstate > nano-particles. Compared with the recently reported results obtained on Ce-based catalysts and other metal oxide catalysts, WO_x/CeO₂ catalysts with monotungstate present the reduced Ea and the increased activity for CB and DCB oxidation (Table S2). Moreover, for the oxidation of other CVOCs, such as 1,2-dichloroethane (1,2-DCE), dichloromethane (DCM) and 1,1,2-trichloroethylene (TCE), 1.0 W presents high activity and selectivity for CO₂ and HCl, with T₉₀ of 281, 310 and 324 °C, respectively, in the feed composed of 1000 ppm reactant and 10% O₂ at GHSV = 60000 h⁻¹ (Fig. S7). This universality of WO_x/CeO₂ catalysts for the oxidation of CVOCs is a synergism of strong acidity, surface oxygen and high resistance to Cl poisoning.

3.3. Distribution of products

TPSR experiments present that the products for CB oxidation are composed of CO/CO₂, HCl, Cl₂, trace DCB and B (Fig. S8). In the parallel kinetic reactions, as shown in Fig. 5, these products were analysed on line (Fig. 7A). The formation of Cl₂ is not significant until 325 °C. As known, Ce-based catalysts are active for Deacon reaction [39]. The highest activity is observed over 1.0 W with 18% selectivity for Cl₂ at 450 °C, where 6.5 W presents as low as 2.8% selectivity (Fig. 7A insert). For chlorination products, 1,2-DCB and 1,4-DCB (DCBs) are detected at 225 °C or higher with a quite similar distribution (Fig. S9), suggesting that the chlorination of CB occurs via a classical aromatic electrophilic substitution mechanism [38]. Over 1.0 W, 2.4 W, 3.4 W and 6.5 W, a similar distribution of DCBs at 250–350 °C is observed with the highest selectivity below 12% (the maxima of 56.2, 34.8, 22.3 and 12.7 ppm, respectively). When the conversion approaches 90%, almost no DCBs can be detected (Fig. 7A). For CeO₂, 0.24 W and 0.5 W, DCB distribution becomes broad and DCBs cannot disappear until 450 °C. The highest selectivity increases to about 16%. According to the fact that an initial temperature for DCB formation is much lower than that for Deacon, it can be considered that the adsorbed Cl species is responsible for CB chlorination. The highest selectivity for DCBs increase linearly with Cl deposition obtained from XPS analyses for the used catalysts (Fig. 7B). Especially pointed out, further chlorination product, trichlorobenzene products such as 1,3,5-TCB and 1,2,4-TCB (TCBs) are observed only over CeO₂ at 290–450 °C with the highest selectivity of 0.8%. In the case of 1,2-DCB oxidation, the chlorination occurs in 225–325 °C, and the highest selectivity for TCBs decreases from 21% for CeO₂ to 10% or

lower. Less chlorination occurs over 3.4 W and 6.5 W (Fig. S10), whose surfaces are covered by WO_x. Obviously, chlorination occurs on the sites of CeO₂ far from WO_x, and probably, the defective sites are active for chlorination. As reported, the formation of oxychlorides could be responsible for chlorination [40]. The positively charged Cl species needed for aromatic electrophilic substitution can be produced from oxychlorides, because of oxygen's higher electronegativity. Indeed, the selectivity for DCBs increases gradually with the increase in [O₂] over CeO₂, 1.0 W and 6.5 W (Fig. S11). The CO₂ selectivity is in a range of 70–80% for WO_x/CeO₂ catalysts. CeO₂ presents CO₂ selectivity of 80% or higher. The formation of B should be involved in both the break of C-Cl bond of CB and the nucleophilic attack of hydride from formaldehyde or formate species (see *in situ* FT-IR). Similarly, CB and B were detected in the oxidation of 1,2-DCB.

3.4. The stability of WO_x/CeO₂ catalysts

WO_x/CeO₂ catalysts were evaluated kinetically on the feed stream containing 1000 ppm CB and 10% O₂/N₂ at 250 °C at GHSV of 60,000 h⁻¹ (Fig. 8). Pure CeO₂ deactivates completely within 150 min, as previously reported [7]. Cl could be easily adsorbed on oxygen vacancy [10] or substitute for surface oxygen or basic lattice oxygen on the surface of CeO₂ [11]. Similarly, 0.24 W, 0.5 W and 1.0 W, uncovered completely by WO_x, present a part deactivation for the first 100 min, which should be attributed to Cl strong adsorption on CeO₂ not contacted with WO_x. There appears an induction of 150 min for 1.0 W, 2.4 W and 3.4 W, within which the conversion increases to a significant extent. This phenomenon reflects the reconstruction of surface. Raman spectra of the used 2.4 W for 10 h shows that the band at 977 cm⁻¹ ascribed to monoxo O = W(O-Ce)₄ becomes strong, while the band at 958 cm⁻¹ to dioxo (O=)₂W(O-Ce)₂, weak (Fig. S12), indicating that the transform from (O=)₂W(O-Ce)₂ to O = W(O-Ce)₄ occurs to some extent during the reaction. The reconstruction of dioxo (O=)₂W-Ti into monoxo O = W-Ti was found during raising temperature [41]. This result implies that monoxo monotungstate is more effective for promoting the activity of CeO₂. It was found that the dioxo monotungstate could be evolved into monoxo monotungstate at 250~300 °C, such as in the case of (O=)₂W(O-Ti)₂ [41]. For 6.5 W, there appears no obvious induction, indicating that excess W loading leads to no available exposed Ce to form new W-O-Ce. The TOF_w (Table 4) for 0.5 W, 1.0 W, 2.4 W and 3.4 W after the reaction for 1000 min increases by 13.5%, 30%, 27% and 23%, compared with that for the fresh catalysts, depending on the transformation of dioxo monotungstate. 1.0 W possesses the most dioxo monotungstate, and obtains the highest increase in TOF_w. Raising temperature to 350 °C in the feed containing 3000 ppm [CB], stable conversion over 1.0 W maintains at 90% for 1000 min. 6.5 W presents 42% conversion. A large difference in conversion between 1.0 W and 6.5 W is probably caused by the hindrance of W-O-W or WO₃ nano-particle between the sites for CB adsorption and surface oxygen from CeO₂. The product distributions show that over 0.24 W, 0.5 W and 1.0 W, DCB increases within the first 120 min, and then maintains constant, indicating that chlorination on pure CeO₂ can be promoted by the increase in Cl disposition. XPS analyses for the used catalysts shows that with W loading, the loss of surface oxygen becomes small, and Cl deposition decreases (Table 3), confirming the substitution of Cl for surface oxygen. *In situ* FT-IR (see later section) shows the adsorbed CB species can be oxidized by lattice oxygen at 250 °C, where the deactivation of CeO₂ is complete, indicating that the substitution of Cl for surface lattice oxygen should occur.

3.5. The effect of H₂O and CO₂

In wet feed containing 5% V/V water, the conversion at 200 °C over CeO₂ and 1.0 W increases significantly (Fig. 9), which is mainly ascribed to the promotion of Cl removal by water [42]. However, the negative effect increases at 250 °C or higher. T₉₀ for 1.0 W increases

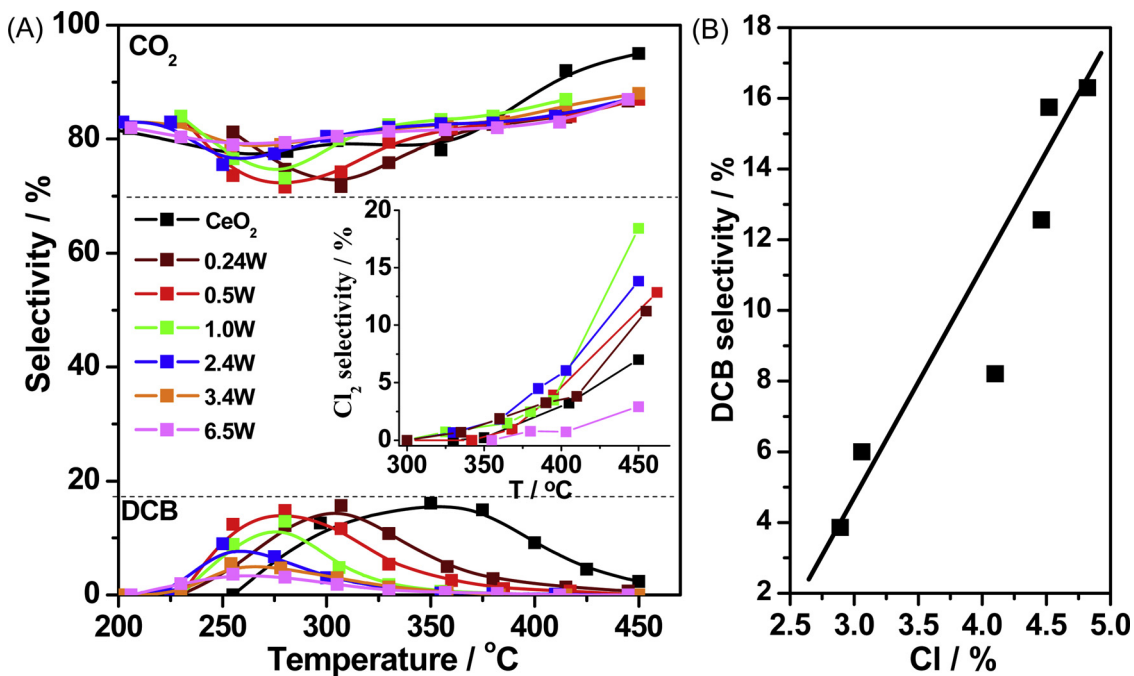


Fig. 7. Distribution of DCB, CO_2 and Cl_2 (insert) during CB oxidation (A) and the highest DCB selectivity vs surface Cl content (B) over WO_x/CeO_2 catalysts; the reaction condition as described in Fig. 5.

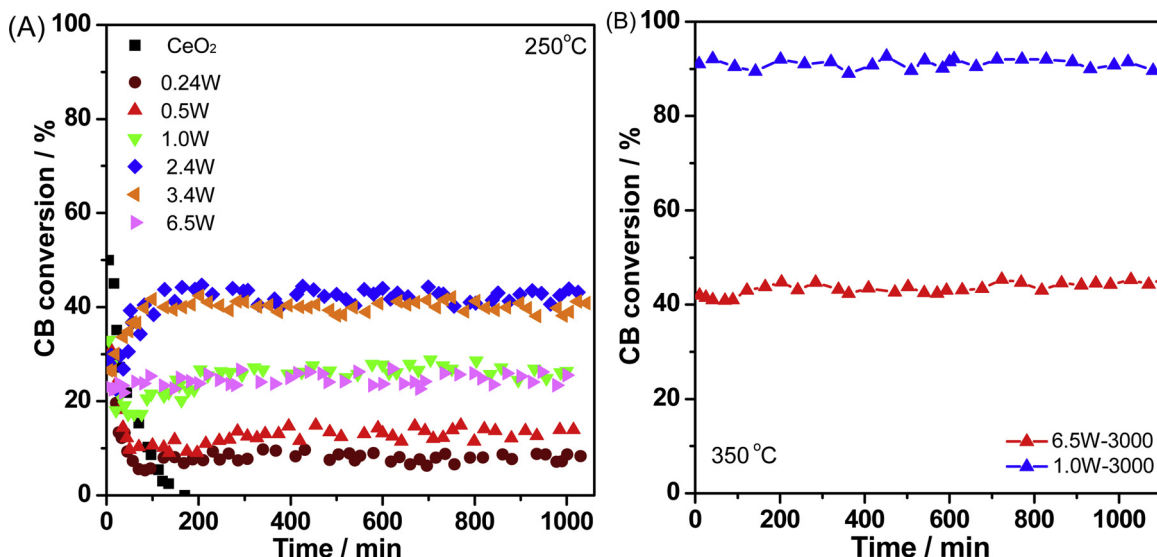


Fig. 8. The activity for CB catalytic combustion over WO_x/CeO_2 catalysts on stream feed at 250 °C (1000 ppm CB) and 350 °C (3000 ppm CB); other gas composition: 10% O_2 and N_2 balance; GHSV: 60,000 h⁻¹; catalyst amount: 200 mg.

from 350 to 405 °C, and the conversion cannot reach 90% over CeO_2 within the experimental temperature. The conversion curve over 1.0 W is similar to that over CeO_2 in dry feed. OH^- from the dissociated water competes with oxygen for adsorption sites as if Cl species does over CeO_2 in dry feed. Lykhach et al. found the existing of hydroxyl groups on CeO_2 at 700 K in SRPES spectra [43]. Strong adsorption of water over CeO_2 makes the formation of surface oxygen rather difficult. Amiridis et al. found that on $\text{V}_2\text{O}_5/\text{TiO}_2$ catalysts, water was favorable at low temperature for the removal of Cl species and C species on the surface during 1,2-DCB oxidation, but it inhibited the reaction at high temperature through water adsorption on the active sites [42]. There is still a significant difference in wet activity between 1.0 W and CeO_2 without surface oxygen and Cl deposition, verifying that the reaction pathway in wet feed is not the oxidation of adsorbed CB by gas oxygen. The adsorbed CB species, such as phenolate, which is formed easily on

the surface covered by hydroxyl groups, can be hydrated on acidic sites. As expected, 1.0 W with abundant strong acid sites is more active for hydration than CeO_2 . The products are mainly composed of CO , HCl and H_2O . Chlorination is greatly inhibited and the amount of DCBs is below 5 ppm (Fig. S13). In order to verify the effect of surface oxygen on wet activity, CeO_2 and 1.0 W supported by 0.5 wt.%Pt (which is resistance to water) were investigated in wet feed. As known, in the presence of water, gas oxygen can be adsorbed and activated on Pt species [44], which leads to the formation of active surface oxygen species needed for reaction. Indeed, 0.5 wt.%Pt/ CeO_2 or 0.5 wt.%Pt/1.0 W shows a similar activity in wet and dry feed, while the addition of 0.5 wt.%Pt cannot increase the dry activity of CeO_2 or 1.0 W to a significant extent, indicating that the availability of surface oxygen is critical to CB wet oxidation over WO_x/CeO_2 catalysts. During stability test in wet feed, 1.0 W presents stable wet activity with the conversion

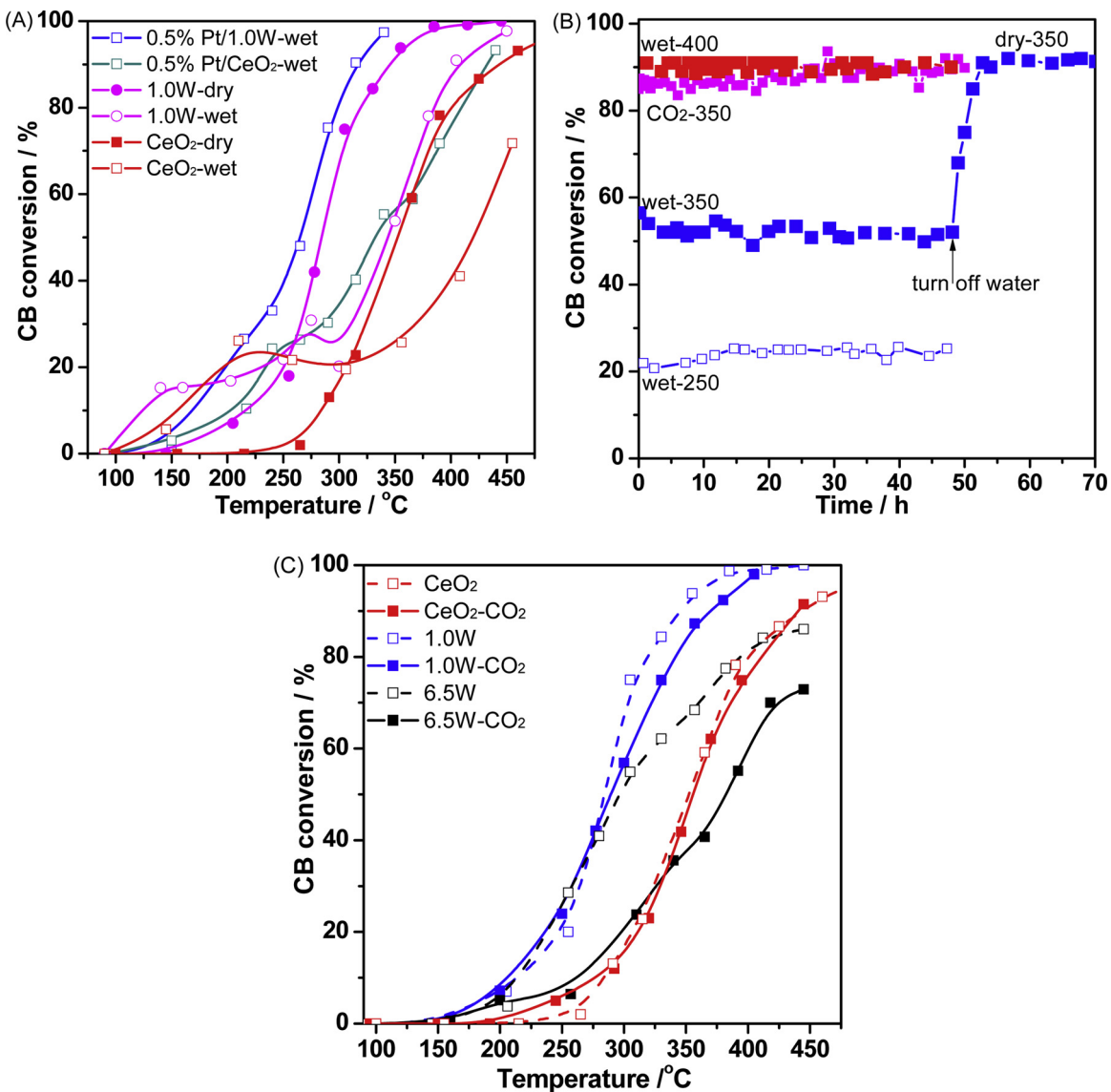


Fig. 9. The activity in wet feed (containing 5% water) over 0.5%Pt/1.0 W, 0.5%Pt/CeO₂, 1.0 W and CeO₂ (A); stable activity of 1.0 W (B) at different temperature in wet feed or 5% CO₂ feed, in which the activity of CeO₂, 1.0 W and 6.5 W (C); gas compositions; 1000 ppm CB, 10% O₂ and N₂ balance; GHSV: 60,000 h⁻¹; catalyst amount: 200 mg.

at 250, 350 and 400 °C of 22%, 52% and 90%, respectively for 50 h without substantial change (Fig. 9B). At 50 h, turning off water at 350 °C, the conversion over 1.0 W can restore quickly to the level in dry feed, about 90% (Fig. 9B). These results indicate that W-O-Ce structure is stable in the presence of water. Additionally, the effect of the addition of 5% CO₂ in the feed on the activity of 1.0 W is observed only at high temperature to a small extent (Fig. 9C), and T₉₀ increases from 343 to 368 °C at which the stability maintains at least for 50 h (Fig. 9B). For 6.5 W, the conversion curve shifts greatly to high temperature, which is similar to the cases of 0.7% [O₂] (Fig. S5A), indicating that CO₂ occupies the sites probably involving with the adsorption of oxygen.

3.6. FT-IR spectra

3.6.1. CB adsorption

The samples were treated at 450 °C by flowing Ar for 2 h in order to remove surface oxygen species with subsequent exposure to 1000 ppm CB/Ar to saturation at 250 °C, and then to flowing Ar for 0.5 h. FT-IR spectra for all catalysts exhibit the bands at 1580, 1477 and 1445 cm⁻¹ (Fig. 10A), which is ascribed to the C=C degenerate stretching

vibration of benzene ring [45]. No any band appears on the spectrum of pure WO₃, (Fig. S14), indicating that the sites for CB adsorption are not related to W—O—W species. For CeO₂ and 0.24 W, the observed bands at 1296, 1273 and 1240 cm⁻¹ are ascribed to C—O stretching vibration of phenolate, of which the second band is split into 1273 and 1265 cm⁻¹ for 0.5 W, and shifts to 1265 cm⁻¹ with further increasing W content. Generally, chlorine atom can be abstracted by Lewis acid sites following attack by basic nucleophilic oxygen (O²⁻) or hydroxyl group to form phenolate. In region of 3650–3710 cm⁻¹, there appear several negative bands. At the same time, a broad positive band between 3600 and 3540 cm⁻¹ (Fig. S15) can be observed, suggesting that the surface hydroxyl groups interact with the adsorbed CB molecules through the formation of weak hydrogen-bonded groups (Cl···HO) [45,46]. The difference in frequency for the band around 1265 cm⁻¹ probably results from basic lattice oxygen (O²⁻) of Ce—O surrounded by Ce—O—Ce and Ce—O—W. The bands around 1265 cm⁻¹ present the change in intensity similar to that of their acidity, indicating that the formation of phenolates is related to the acid-base pair [47]. DFT calculations showed that VO_x/CeO₂ catalysts with more Lewis acid sites is more favorable than pure CeO₂ for the adsorption of CVOCs [10]. The formation of polytungstate

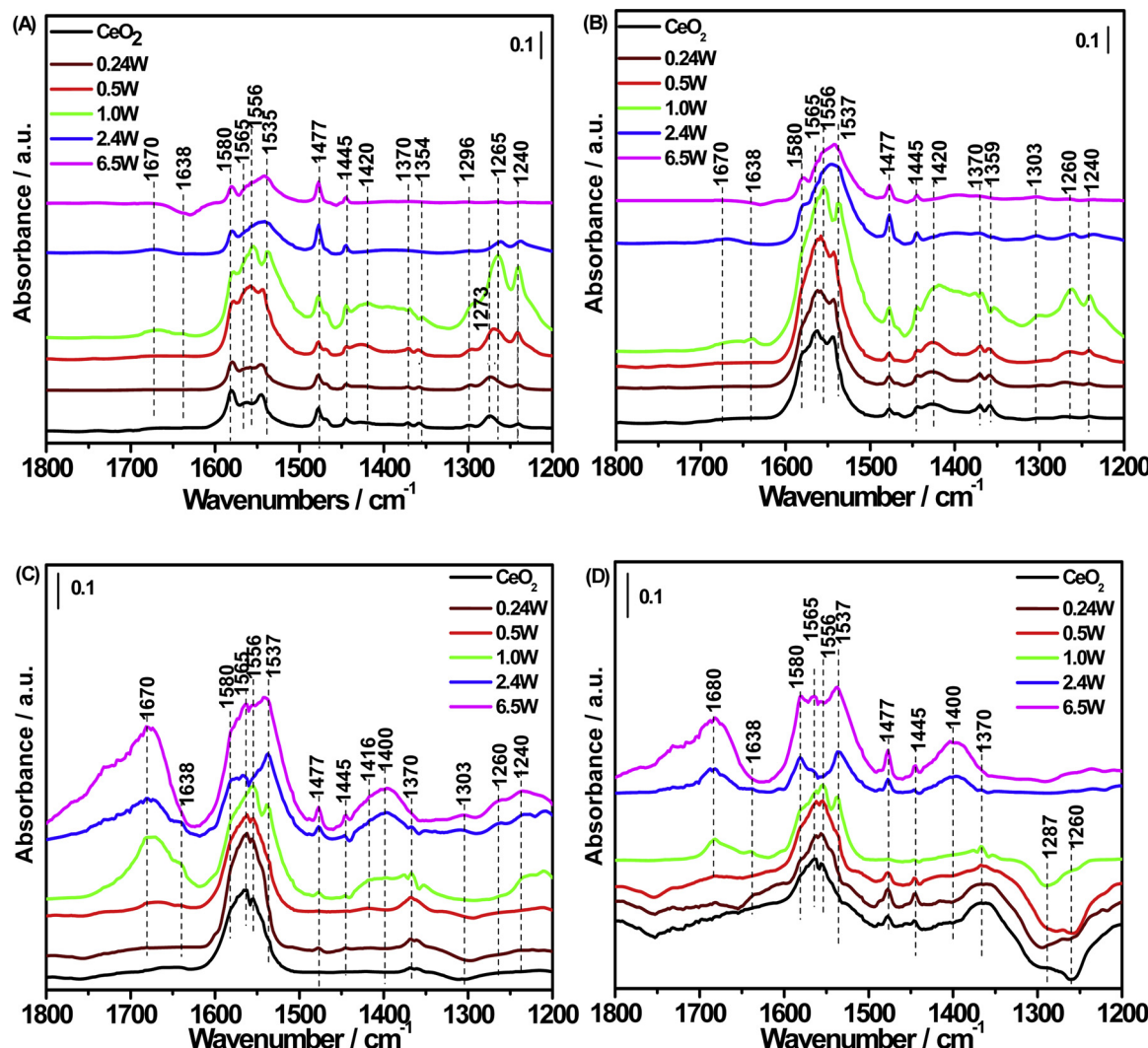


Fig. 10. *In situ* DRIFT in 1200–1800 cm⁻¹ region for WO_x/CeO₂ catalysts degassed after the treatment with Ar stream at 450 °C following the adsorption in 1000 ppm CB/Ar at 250 °C (A) and 300 °C (B) and after the treatment with 10%O₂/Ar stream at 450 °C following the oxidation in 1000 ppm CB/10%O₂/Ar at 250 °C (C) and 300 °C (D).

W–O–W species can decrease the acid-base pair, and thus 6.5 W presents the weakest formation of phenolates. The strongest bands obtained on 1.0 W is owing to its possessing most acid-base pairs. The bands at 2880, 1535, 1370 and 1354 cm⁻¹, which is ascribed to C–H stretching, COO- asymmetric stretching, C–H deformation and COO-symmetric stretching vibrations of stable formate ions [48]. There appear other carboxylate (the bands at 1535–1565 and 1354–1370 cm⁻¹) and bidentate carbonate (the bands at 1556–1565 and 1400–1420 cm⁻¹). Raising temperature up to 300 °C, the bands for partial oxidation intermediates become strong significantly, due to the enhanced oxidation of phenolate (Fig. 10B). At the same time, the bands at 2340 and 2093 cm⁻¹, ascribed to CO₂ and CO, become perceptible (Fig. S18). Here, the formation of partial oxidation intermediates and CO_x involves surface lattice oxygen, because neither gas oxygen nor surface oxygen species exists.

3.6.2. CB oxidation

The recorded spectra of the catalysts after treated by the feed containing oxygen at 250 °C (Fig. 10C) show still the bands ascribed to the adsorbed CB and partial oxidation intermediates. It should be noted that on the spectrum of 6.5 W, the bands around 1265 cm⁻¹ are promoted significantly in the presence of gas oxygen (Fig. 10C). One H₂O molecule produced during oxidation reacts with several O=W groups

to form hydroxyl groups with Brønsted acidity, on which both CB adsorption and Cl abstraction can be promoted. For CeO₂, 0.24 W, 0.5 W and 1.0 W, there appears new negative band at 1240–1300 cm⁻¹, whose intensity decreases with W loading (Fig. 10C). Combining the results from Raman spectra (1175 cm⁻¹), this band is probably ascribed to super oxygen (O₂[·]). That is to say, Cl produced during CB decomposition can substitute O₂[·] from bare CeO₂, which is consistent with the deactivation in the stability test at 250 °C. Additionally, on the spectra of 1.0 W, 2.4 W and 6.2 W, new strong bands appear at 1750–1650 and 1400–1416 cm⁻¹, which can be ascribed to ν(C=O) and δ_{as}(CH₃) of acetaldehyde [49]. Moreover, the band at 1638 cm⁻¹ is observed for 1.0 W and 2.4 W, accompanied by two significant peaks at 1416 and 1303 cm⁻¹. These three peaks are attributed to a surface enolic species with resonance structure of acetaldehyde, which is confirmed by the presence of C=C and –CH– bonds (the bands at 2936 and 2845 cm⁻¹) [50]. In the absence of gas oxygen, or for the catalysts with less or no Brønsted acid site, such as CeO₂, 0.24 W and 0.5 W, almost no acetaldehyde is formed. In fact, there appears a new negative band of acidic hydroxyl group at 3646 cm⁻¹ (Fig. S16) over 1.0 W, 2.4 W and 6.5 W. It can be considered that the formation of acetaldehyde is a synergism between Brønsted acid sites and gas oxygen (there is no more available surface oxygen for 6.5 W). At 300 °C or higher, the band at 1670 cm⁻¹ becomes weak quickly over 1.0 W and 2.4 W, while for 6.5 W, still

maintains considerably high intensity (Fig. 10D), indicating that surface oxygen is responsible for the complete oxidation of acetaldehyde. 6.5 W with abundant O₂²⁻ species probably is not highly active for the oxidation of adsorbed acetaldehyde. In fact, the amount of active surface oxygen species for 6.5 W is comparable to that for 2.4 W. The formation of polytungstate W–O–W can separate the adsorbed acetaldehyde and O₂²⁻. For 0.24 W and 0.5 W, abundant surface oxygen in interface between monoxo O = W(O-Ce)₄ and CeO₂ can oxidize effectively partial oxidation intermediates. A similar phenomenon is observed on FT-IR spectra of 1,2-DCB oxidation at 300 °C over 1.0 W and 6.5 W (Fig. S17). From the all above results, the reaction pathway on 2.4 W and 1.0 W with high activity can be described as following: CB molecules adsorb on the surface through the abstraction of chlorine atom by Lewis acidic sites following by attack of basic O₂²⁻ species to form phenolate. Reactive acetaldehyde and its resonance isomer enolic species can be promoted greatly with a synergism of Brönsted acid and gas oxygen. Then, these two intermediates are oxidized by surface oxygen species into carboxylates or carbonates. Finally, oxygenate species are further oxidized to CO_x.

4. Conclusion

WO_x/CeO₂ catalysts with various loadings of WO_x (0.75–12 wt%) prepared by wet impregnation method were characterized by XRD, N₂ isothermal adsorption and desorption, Raman, XPS, H₂-TPR, O₂-TPD and NH₃-TPD. The experimental results show that CeO₂ exists as a form of cubic fluorite structure. WO_x presents mono-tungstate monoxo O = W(O-Ce)₄ and dioxo (O =)₂W(O-Ce)₂, polytungstate, nano-particles, depending on W loading. W-O-Ce is formed as a result of interaction between WO_x and CeO₂, which decreases surface O₂²⁻ and O-species, while promotes the reducibility and acidity of WO_x/CeO₂ catalysts. While peroxy-like O₂²⁻ increases significantly for the catalysts with W density of 2.4 W atom/nm² or higher. CeO₂ species in contact with WO₃ clusters is more reducible than pure CeO₂, and the reduction of WO₃ into WO₂ would be promoted by an interaction between WO₃ and CeO₂. Both the W = OH sites considered as Brönsted acid sites and highly unsaturated W⁶⁺ as strong Lewis acid site are promoted by WO₃ contacted with CeO₂.

In CB oxidation, WO_x/CeO₂ catalysts present excellent activity, stability and selectivity for CO_x, especially for the catalysts with monotungstate WO_x. Although the CeO₂ species contacted with WO_x possesses the decreased active O²⁻ and O-species, high resistance to Cl species can maintain the effectiveness of surface oxygen and promote the transformation of gas oxygen into surface oxygen, which leads to the decreased in Ea. TOF_W based on the mol of transformed CB and DCB per second per W atom is proportional to surface oxygen, and W-O-Ce around by more surface oxygen is highly active. For the oxidation of other CVOCs, such as 1,2-DCE, DCM and TCE, 1.0 W presents high activity and selectivity for CO₂ and HCl, with T₉₀ of 281, 310 and 324 °C, respectively. Product analyses show that W loading greatly inhibits the chlorination of benzene ring. The stability tests for 1000 min at 250 °C show that there is an induction within which the activity increases significantly, and the corresponding reconstruction, the transform of dioxo (O =)₂W(O-Ce)₂ into monoxx O = W(O-Ce)₄ is observed, which increases the number of W-O-Ce species. Pt promotes wet stable activity through the increase in surface oxygen. W-O-Ce species is stable in wet feed. 5% CO₂ in feed has no effect on the catalysts with monotungstate WO_x, while on 6.5 W, the activity is inhibited, probably through the decrease in availability of surface oxygen. *In situ* FT-IR shows that the adsorbed CB species can be oxidized by surface lattice oxygen to form phenolate, carboxylates and carbonate. However, the presence of gas oxygen promotes the formation of acetaldehyde on the WO_x/CeO₂ catalysts with Brönsted acidity. The partial oxidation intermediates can be oxidized into CO₂, HCl and H₂O by surface oxygen.

Acknowledgments

We would like to acknowledge the National Key Research and Development Program of China (no. 2016YFC0204300) and National Natural Science Foundation of China (no. 21477036 and 21777043).

Appendix A. Supplementary data

Supplementary material related to this article can be found, in the online version, at doi:<https://doi.org/10.1016/j.apcatb.2018.12.055>.

References

- [1] A.A. Meharg, D. Osborn, Dioxins released from chemical accidents, *Nature* 375 (1995) 353–354.
- [2] J. Chen, X. Chen, X. Chen, W.J. Xu, Z. Xu, H.P. Jia, J. Chen, Homogeneous introduction of CeO_y into MnO_x-based catalyst for oxidation of aromatic VOCs, *Appl. Catal. B: Environ.* 224 (2018) 825–835.
- [3] A. Khaleel, A. Al-Nayli, Supported and mixed oxide catalysts based on iron and titanium for the oxidative decomposition of chlorobenzene, *Appl. Catal. B: Environ.* 80 (2008) 176–184.
- [4] T. Cai, H. Huang, W. Deng, Q.G. Dai, W. Liu, X.Y. Wang, Catalytic combustion of 1,2-dichlorobenzene at low temperature over Mn-modified Co₃O₄ catalysts, *Appl. Catal. B: Environ.* 166–167 (2015) 393–405.
- [5] C. Gannoun, A. Turki, H. Kochkar, R. Delaigle, P. Eloy, A. Ghorbel, E.M. Gaigneaux, Elaboration and characterization of sulfated and unsulfated V₂O₅/TiO₂ nanotubes catalysts for chlorobenzene total oxidation, *Appl. Catal. B: Environ.* 147 (2014) 58–64.
- [6] A.M. Padilla, J. Corella, J.M. Toledo, Total oxidation of some chlorinated hydrocarbons with commercial chromia based catalysts, *Appl. Catal. B: Environ.* 22 (1999) 107–121.
- [7] X.Y. Wang, Q. Kang, D. Li, Catalytic combustion of chlorobenzene over MnO_x-CeO₂ mixed oxide catalysts, *Appl. Catal. B: Environ.* 86 (2009) 166–175.
- [8] Q.G. Dai, X.Y. Wang, G.Z. Lu, Low-temperature catalytic combustion of trichloroethylene over cerium oxide and catalyst deactivation, *Appl. Catal. B: Environ.* 81 (2008) 192–202.
- [9] W. Deng, Q.G. Dai, Y.J. Lao, B.B. Shi, X.Y. Wang, Low temperature catalytic combustion of 1,2-dichlorobenzene over CeO₂-TiO₂, mixed oxide catalysts, *Appl. Catal. B: Environ.* 181 (2016) 848–861.
- [10] Q.G. Dai, L.L. Yin, S.X. Bai, W. Wang, X.Y. Wang, X.Q. Gong, G.Z. Lu, Catalytic total oxidation of 1,2-dichloroethane over VO_x/CeO₂ catalysts: further insights via isotopic tracer techniques, *Appl. Catal. B: Environ.* 182 (2016) 598–610.
- [11] H. Huang, Y.F. Gu, J. Zhao, X.Y. Wang, Catalytic combustion of chlorobenzene over VO_x/CeO₂ catalysts, *J. Catal.* 326 (2015) 54–68.
- [12] Q.Q. Huang, Z.H. Meng, R.X. Zhou, The effect of synergy between Cr₂O₃-CeO₂ and USY zeolite on the catalytic performance and durability of chromium and cerium modified USY catalysts for decomposition of chlorinated volatile organic compounds, *Appl. Catal. B: Environ.* 115–116 (2012) 179–189.
- [13] M. Iwasaki, K. Dohmae, Y. Nagai, E. Sudo, T. Tanaka, Experimental assessment of the bifunctional NH₃-SCR pathway and the structural and acid-base properties of WO₃ dispersed on CeO₂ catalysts, *J. Catal.* 359 (2018) 55–67.
- [14] M. Iwasaki, E. Iglesias, Mechanistic assessments of NO oxidation turnover rates and active site densities on WO₃-promoted CeO₂ catalysts, *J. Catal.* 342 (2016) 84–97.
- [15] L. Chen, D. Weng, Z.C. Si, X.D. Wu, Synergistic effect between ceria and tungsten oxide on WO₃-CeO₂-TiO₂ catalysts for NH₃-SCR reaction, *Prog. Nat. Sci.: Mater. Int.* 22 (2012) 265–272.
- [16] G. Qi, R. Yang, R. Chang, MnO_x-CeO mixed oxides prepared by co-precipitation for selective catalytic reduction of NO with NH₃ at low temperatures, *Appl. Catal. B: Environ.* 51 (2004) 93–106.
- [17] A.S. Mamede, E. Payen, P. Grange, G. Poncelet, A. Ion, M. Alifanti, V.I. Părvulescu, Characterization of WO_x/CeO₂ catalysts and their reactivity in the isomerization of hexane, *J. Catal.* 223 (2004) 1–12.
- [18] Y. Peng, K.Z. Li, J.H. Li, Identification of the active sites on CeO₂-WO₃ catalysts for SCR of NO_x with NH₃: an *in situ* IR and Raman spectroscopy study, *Appl. Catal. B: Environ.* 140–141 (2013) 483–492.
- [19] M.N. Taylor, W. Zhou, T. Garcia, B. Solsona, A.F. Carley, C.J. Kiely, S.H. Taylor, Synergy between tungsten and palladium supported on titania for the catalytic total oxidation of propane, *J. Catal.* 285 (2012) 103–114.
- [20] J.A. Dean, Lange's Handbook of Chemistry, fifteenth ed., McGraw-Hill Book Co., New York, 1999.
- [21] Q.G. Dai, H. Huang, Y. Zhu, W. Deng, S.X. Bai, X.Y. Wang, G.Z. Lu, Catalysis oxidation of 1,2-dichloroethane and ethyl acetate over ceria nanocrystals with well-defined crystal planes, *Appl. Catal. B: Environ.* 117–118 (2012) 360–368.
- [22] A. Joshi, A. Rammohan, Y. Jiang, S. Ogundumini, Density functional theory (DFT) study of the interaction of ammonia with pure and tungsten-doped ceria, *J. Mol. Struct. (Thiochem)* 912 (2009) 73–81.
- [23] D.S. Aidhy, B. Liu, Y. Zhang, W.J. Weber, Strain-induced phase and oxygen-vacancy stability in ionic interfaces from first-principles calculations, *J. Phys. Chem. C* 118 (2014) 30139–30144.
- [24] X. Carrier, J.B. Caillerie, J.F. Lambert, M. Che, The support as a chemical reagent in the preparation of WO_x/γ-Al₂O₃ catalysts: formation and deposition of alumino-tungstic heteropoly-anions, *J. Am. Chem. Soc.* 121 (1999) 3377–3381.

- [25] M. Daniel, S. Loridan, Probing reoxidation sites by *in situ* Raman spectroscopy: differences between reduced CeO₂ and Pt/CeO₂, *J. Raman Spectrosc.* 43 (2012) 312–319.
- [26] E.I. Ross-Medgaarden, I.E. Wachs, Structural determination of bulk and surface tungsten oxides with uv–vis diffuse reflectance spectroscopy and Raman spectroscopy, *J. Phys. Chem. C* 111 (2007) 15089–15099.
- [27] Y.Y. He, M.E. Ford, M.H. Zhu, Q.C. Liu, Z.L. Wu, I.E. Wachs, Selective catalytic reduction of NO by NH₃ with WO₃-TiO₂ catalysts: influence of catalyst synthesis method, *Appl. Catal. B: Environ.* 188 (2016) 123–133.
- [28] T. Kim, A. Burrows, C.J. Kiely, I.E. Wachs, Molecular/electronic structure-surface acidity relationships of model-supported tungsten oxide catalysts, *J. Catal.* 246 (2007) 370–381.
- [29] S. Ghosh, S.S. Acharyya, T. Sasaki, R. Bal, Room temperature selective oxidation of aniline to azoxybenzene over a silver supported tungstenoxide nanostructured catalyst, *Green Chem.* 17 (2015) 1867–1876.
- [30] S. Sathasivam, D.S. Bhachu, Y. Lu, N. Chadwick, S.A. Alhabaiti, A.O. Alyoubi, S.N. Basahel, C.J. Carmalt, I.P. Parkin, Tungsten doped TiO₂ with enhanced photocatalytic and optoelectrical properties via aerosol assisted chemical vapor deposition, *Sci. Rep.* 5 (2015) 1–10.
- [31] Z.R. Ma, D. Weng, X.D. Wu, Z.C. Si, Effects of WO_x modification on the activity, adsorption and redox properties of CeO₂ catalyst for NO(x) reduction with ammonia, *J. Environ. Sci.* 24 (2012) 1305–1316.
- [32] H. Huang, Q.G. Dai, X.Y. Wang, Morphology effect of Ru/CeO₂ catalysts for the catalytic combustion of chlorobenzene, *Appl. Catal. B: Environ.* 158–159 (2014) 96–105.
- [33] J. Macht, C.D. Baertsch, M. May-Lozano, S.L. Soled, Y. Wang, E. Iglesia, Support effects on Brønsted acid site densities and alcohol dehydration turnover rates on tungsten oxide domains, *J. Catal.* 227 (2004) 479–491.
- [34] Y. Nagai, K. Dohmae, Y.F. Nishimura, H. Kato, H. Hirata, N. Takahashi, Operando XAFS study of catalytic NO reduction over Cu/CeO₂: the effect of copper-ceria interaction under periodic operation, *Phys. Chem. Chem. Phys.* 15 (2013) 8461–8465.
- [35] C. Li, K. Domen, K. Maruya, T. Onishi, Dioxygen adsorption on well-outgassed and partially reduced cerium oxide studied by FT-IR, *J. Am. Chem. Soc.* 111 (1989) 7683–7687.
- [36] W.P. Shan, F.D. Liu, H. He, X.Y. Shi, C.B. Zhang, A superior Ce-W-Ti mixed oxide catalyst for the selective catalytic reduction of NO_x with NH₃, *Appl. Catal. B: Environ.* 115–116 (2012) 100–106.
- [37] Y. Dai, X.Y. Wang, Q.G. Dai, D. Li, Effect of Ce and La on the structure and activity of MnO_x catalyst in catalytic combustion of chlorobenzene, *Appl. Catal. B: Environ.* 111–112 (2012) 141–149.
- [38] M.V. Ganduglia-Pirovano, C. Popa, J. Sauer, H. Abbott, A. Uhl, M. Baron, D. Stacchiola, O. Bondarchuk, S. Shaikhutdinov, H.J. Freund, Role of ceria in oxidative dehydrogenation on supported vanadia catalysts, *J. Am. Chem. Soc.* 132 (2010) 2345–2349.
- [39] A.P. Amrute, C. Mondelli, M. Moser, G. Novell-Leruth, N. López, D. Rosenthal, R. Farra, M.E. Schuster, D. Teschner, T. Schmidt, J. Pérez-Ramírez, Performance, structure, and mechanism of CeO₂ in HCl oxidation to Cl₂, *J. Catal.* 286 (2012) 287–297.
- [40] R.W. van den Brink, R. Louw, P. Mulder, Formation of polychlorinated benzenes during the catalytic combustion of chlorobenzene using a Pt/γ-Al₂O₃, catalyst, *Appl. Catal. B: Environ.* 16 (1998) 219–226.
- [41] A. Tribalis, G.D. Panagiotou, G. Tsilomelekis, A.G. Kalampounias, K. Bourikas, C. Kordulis, S. Boghosian, A. Lycourghiotis, Temperature-dependent evolution of the molecular configuration of oxo-tungsten(VI) species deposited on the surface of titania, *J. Phys. Chem. C* 118 (2014) 11319–11332.
- [42] C.E. Hetrick, F. Patcas, M.D. Amiridis, Effect of water on the oxidation of dichlorobenzene over V₂O₅/TiO₂ catalysts, *Appl. Catal. B: Environ.* 101 (2011) 622–628.
- [43] L. Lykhach, V. Johánek, H.A. Aleksandrov, S.M. Kozlov, M. Happel, T. Skála, P.S. Petkov, N. Tsud, G.N. Vayssilov, K.C. Prince, K.M. Neyman, V. Matolín, J. Libuda, Water chemistry on model ceria and Pt/Ceria catalysts, *J. Phys. Chem. C* 116 (2012) 12103–12113.
- [44] L. Gutierrez, A. Boix, J. Petunchi, Effect of Pt on the water resistance of Co-zeolites upon the SCR of NO_x with CH₄, *Catal. Today* 54 (1999) 451–464.
- [45] M. Nagao, Y. Suda, Adsorption of benzene, toluene, and chlorobenzene on titanium dioxide, *Langmuir* 5 (1989) 42–47.
- [46] P. Li, C. He, J. Cheng, C.Y. Ma, B.J. Dou, Z.P. Hao, Catalytic oxidation of toluene over Pd/Co₃AlO catalyst derived from hydrotalcite-like compounds: effects of preparation methods, *Appl. Catal. B: Environ.* 101 (2011) 570–579.
- [47] G.N. Robinson, Q. Dai, A. Freedman, Reactions of halomethanes with γ-alumina surfaces. 2. X-ray photoelectron and temperature-programmed reaction spectroscopic studies, *J. Phys. Chem. B* 101 (1997) 4940–4946.
- [48] G. Busca, V. Lorenzelli, Infrared study of methanol, formaldehyde, and formic acid adsorbed on hematite, *J. Catal.* 66 (1980) 155–161.
- [49] B. Hauchecorne, D. Terrens, S. Verbruggen, J.A. Martens, H.V. Langenhove, K. Demeestere, S. Lenaerts, Elucidating the photocatalytic degradation pathway of acetaldehyde: an FTIR *in situ* study under atmospheric conditions, *Appl. Catal. B: Environ.* 106 (2011) 630–638.
- [50] D.P. Dreoni, D. Pinelli, F. Trifiro, G. Busca, V. Lorenzelli, FT-IR and flow reactor studies on heterogeneously catalyzed gas-phase ammoniation of cyclohexanone, *J. Mol. Catal.* 71 (1992) 111–127.